Full-field 3D measurement of solder pastes using LCD-based phase shifting techniques

by

Hsu-Nan Yen, Du-Ming Tsai and Jun-Yi Yang

Department of Industrial Engineering and Management
Yuan-Ze University, Taiwan, R.O.C.

Correspondence:

Du-Ming Tsai
Department of Industrial Engineering & Management
Yuan-Ze University
135 Yuan-Tung Road
Nei-Li, Tao-Yuan
Taiwan, R.O.C.

Tel: (03) 463-8800
Fax: (03) 463-8907
E-mail: iedmtsai@saturn.yzu.edu.tw

Full-field 3D measurement of solder pastes

using LCD-based phase shifting techniques

Abstract

Quality inspection of deposited solder pastes is critical in surface mounting processes. As SMT component pitches decrease, 3D measurement of solder pastes has become more and more important in ensuring solder joint reliability. Currently, the 3D measurements for solder pastes are mainly performed by laser-based systems. However, they suffer from low inspection speed due to the physical line-scanning process. In this paper, a fast and cost-effective 3D measurement system for deposited solder pastes is proposed. The proposed system uses an LCD-based phase shifting technique to perform full-field 3D measurement of solder pastes with high accuracy. Experiments have shown that the 3D profiling and volume measurement of solder pastes are very efficient and effective with the proposed system. The volume measurement repeatability is in the micrometer range. The processing time of the proposed 3D measurement system for an image of 640×480 pixels is less than 1 second on a typical personal computer.

Keywords: Three-dimensional measurement; Solder paste volume; Printing quality inspection; Phase shifting technique

1. Introduction

Recently, surface mount technology (SMT) has become the dominant assembly technique in the electronics industry. In the SMT process, the interconnection between electronic components and printed circuit boards (PCBs) is realized by solder pastes. The solder paste printing process is a delicate step, which can be easily affected by many manufacturing factors. It has been reported that 52 to 71% of SMT defects are related to the printing process [1-4]. To reduce solder paste defects and save reworking costs, inspecting deposited solder pastes immediately after the stencil printing process is indispensable.

Automatic visual inspection systems are often used to inspect the solder paste printing quality. These optical-based systems are two dimensional (2D), and are capable of measuring the area and position of deposited solder pastes. They can effectively inspect defects such as paste-to-pad offset, solder bridge, solder smear, solder paste absence, and excess/undersized solder area [5-8]. But they are restricted in detecting solder slump and insufficient or excess solder paste volume. Such defects need three-dimensional (3D) measurement of surface profiles and the volume of the solder pastes. As the leads of SMT components become dense, 3D measurement will become more and more important in the quality inspection of solder pastes [4,9,10].

Three dimensional measurement of deposited solder pastes not only can detect the 3D defects, but also can improve the stencil printing process with feedback volume information [11,12]. Currently, nondestructive 3D measurement of deposited solder pastes is mainly performed by laser scanning systems [9-16]. These systems first project a laser line onto solder pastes and detect light reflection with optical

sensors. Height data of inspected solder pastes are then acquired using the optical triangular method. The surface profile and volume of inspected solder pastes must be obtained with a sufficient number of height data points. Since only one line can be measured at a time, the laser head or the worktable must be physically moved to construct the whole 3D profile of the solder pastes. This results in slow measurement speed and the need for high-precision motion control. Any vibration occurring in the movement makes the 3D measurement imprecise. In addition, the measuring accuracy of laser scanning systems is greatly affected by laser beam spot reflection and stray light.

Phase measuring methods have been applied to perform 3D profiling of large objects, such as car models, mannequin faces, and plaster models of human teeth [17-19]. In the traditional phase measuring methods, the projected sinusoidal fringe pattern is acquired by the interference of two lasers, and the phase step is obtained by a piezocrystal (PZT) [20-23]. Speckle noise produced by the laser interference may affect the intensity distribution of projected fringes, and the PZT cannot accurately shift the phase step due to its nonlinear property. The measuring accuracy is reduced accordingly.

The required sinusoidal fringe pattern in phase measuring methods can also be created by projecting an image of a white light illuminated sinusoidal transmission grating [24,25]. The corresponding phase shifting is obtained by a stepper motor-driven translation stage. However, the movement of a stepper motor-driven translation stage cannot be continuous and precise. Due to the mechanical movement of the translation stage, the measuring accuracy will be affected by vibration, which is the main error source in applying phase shifting techniques.

In this paper, a fast and cost-effective machine vision system with a liquid crystal display (LCD) based phase shifting technique is proposed to perform 3D measurement of deposited solder paste. Different from the line-scanning measurement of laser-based systems, the proposed phase measuring system can provide full-field 3D measurement of deposited solder pastes. The proposed system uses an incoherent light source and a software-controlled LCD grating to project an area of fine sinusoidal fringes on the deposited solder pastes. The projected sinusoidal fringes will be deformed by the surface height variations of the solder pastes. By detecting the deformed sinusoidal fringes, and in combination with phase shifting analysis, full-field and high-precision 3D measurement of solder pastes in a sizable area can be efficiently acquired. Surface profile and volume of deposited solder pastes can be effectively and reliably calculated with much height data obtained from the proposed system.

This paper is organized as follows. Section 2 introduces the 3D measurement principle of phase measuring methods. Section 3 describes the proposed LCD-based phase shifting technique and its implementation for 3D measurement of solder pastes. In section 4, the performance of the proposed system in terms of measurement accuracy and repeatability is first evaluated with a standard 1-*mm* gauge block. Experimental results on 3D measurement of solder pastes and the volume measurement repeatability of the proposed technique are then presented and analyzed. This paper is concluded in Section 5.

2. The principle of phase measuring techniques

The optical geometry of the phase measuring techniques is shown in Figure 1, in which h is the surface height of the measured object. When a sinusoidal fringe pattern is projected onto a 3D object, the surface height $h(x, y)$ of an object at coordinates (x, y) is mapped to a phase function of the deformed intensity fringe pattern, and can be resolved by [20]

$$h(x, y) = \frac{P_o}{2\pi} \tan\theta_p \cdot [\phi_r(x, y) - \phi_o(x, y)] = \frac{P_o}{2\pi} \tan\theta_p \cdot \Delta\phi(x, y) \quad (1)$$

where P_o is the period of sinusoidal grating in the reference plane, θ_p is the angle between the axis of projection and the reference plane, $\phi_r(x, y)$ is the phase value at coordinates (x, y) on the reference plane, $\phi_o(x, y)$ is the phase value at coordinates (x, y) with the presence of an object, and $\Delta\phi(x, y)$ is the phase difference between $\phi_r(x, y)$ and $\phi_o(x, y)$.

Because the values of optical parameters P_o and θ_p are fixed throughout the measuring process, Eq. (1) can be simplified as

$$h(x, y) = k \cdot \Delta\phi(x, y) \quad (2)$$

where $k = \frac{P_o}{2\pi} \tan\theta_p$. Parameter k is a known constant for a given system setup, and can be acquired with a simple system calibration procedure described later in Section 3.3. Calculation of the surface height $h(x, y)$ is now simplified to the determination of the phase difference $\Delta\phi(x, y)$ at each of the coordinates (x, y) on the projection plane.

If a sinusoidal fringe pattern is projected onto a plane, its intensity image $I(x, y)$ can be expressed as

$$I(x, y) = I_b(x, y) + I_m(x, y)\cos\phi(x, y) \tag{3}$$

where $I_b(x, y)$ is the background intensity, $I_m(x, y)$ is the fringe modulation, and $\phi(x, y)$ is the phase value at coordinates (x, y). $I(x, y)$ in Eq. (3) is the known intensity image of the projected sinusoidal fringe pattern obtained from the sensing CCD camera. $I_b(x, y)$, $I_m(x, y)$ and $\phi(x, y)$ are three unknown variables in Eq. (3). To extract the desired phase $\phi(x, y)$, at least three intensity images of different projected sinusoidal fringe patterns are required.

If the phase shifting increment is $\pi/2$ and the four-step phase shifting method is adopted, then the four intensity images of sinusoidal gratings by sequential phase shifting can be formulated as

$$I_n(x, y) = I_b(x, y) + I_m(x, y)\cos[\phi(x, y) + (n-1)\frac{\pi}{2}], \qquad n = 1, 2, 3, 4 \tag{4}$$

By solving the four equations above, the phase $\phi(x, y)$ at coordinates (x, y) can be computed as

$$\phi(x, y) = \tan^{-1}\left[\frac{I_4(x, y) - I_2(x, y)}{I_1(x, y) - I_3(x, y)}\right] \tag{5}$$

The advantage of using the four-step phase shifting method is that a zero value in the denominator in Eq. (5), which may occur in the three-step phase shifting method, can be avoided. The phase $\phi(x, y)$ calculated from Eq. (5) is between $-\pi/2$ and

$\pi/2$, and is not the actual phase value. It cannot be directly used to evaluate the surface height. With the so-called modulo 2π correction [26], the calculated phase $\phi(x,y)$ from Eq. (5) can be extended to the desired range between 0 and 2π. For a pixel with coordinates (x,y), the 2π discontinuities of modulo 2π phase data can be removed by adding 2π to the pixel (x,y) as long as the phase variation of the pixel and its previous adjacent pixel $(x-1,y)$ is larger than π, i.e.,

$$\phi(x,y)=\begin{cases}\phi(x,y)+2\pi & \text{if } \phi(x-1,y)-\phi(x,y)>\pi \\ \phi(x,y) & \text{otherwise}\end{cases} \tag{6}$$

The phase values on the reference plane and on the object, i.e., $\phi_r(x,y)$ and $\phi_o(x,y)$ in Eq. (2), can be obtained according to the forgoing phase unwrapping process. Once the phases that modulate the sinusoidal fringe patterns on the object and on the reference plane are obtained individually, the phase difference $\Delta\phi(x,y)$ can be determined. Then the surface height value of each pixel on the sensed area of the object can be derived from Eq. (2).

3. The proposed 3D measurement system

3.1 The LCD-based phase shifting technique

As aforementioned, there are two essential parts to consider in applying phase measuring technique to perform 3D measurement, i.e., generating the sinusoidal fringe pattern and shifting the generated fringe pattern with accurate phase increment. The LCD panel has uniform optical transparency, and can be software-controlled by connecting it to a personal computer. The unique electro-optical capability of the LCD panel makes it well suited as a controllable sinusoidal transparency grating.

In the proposed system, a sinusoidal fringe pattern is first software-generated and displayed on the LCD panel to form a sinusoidal transparency grating. Let the LCD resolution be R×C. The software-generated fringe pattern in this study is given as follows. For a given column *c*, *c* = 0, 1, 2,…, *C*-1

$$F_n(r,c) = 1 + \sin\{\frac{2\pi}{p}[r + (n-1)\delta]\}, \qquad r = 0, 1, 2,\ldots, R\text{-}1 \tag{7}$$

where $F_n(r,c)$ is the *n*-th phase-shifted normalized intensity for $n = 1$, 2, 3 and 4, which correspond to the fringe patterns of four phase shifting steps; p is the fringe period in pixels; and δ is the phase shifting increment. Owing to the pixel structure of an LCD panel, control parameter δ in Eq. (7) is counted by pixels in the proposed system. In the four-step phase increment of $\pi/2$, δ is therefore given by $p/4$. After illuminating the created sinusoidal transparency grating with collimated incoherent light, the required sinusoidal fringe pattern in the phase measuring method is then obtained. It is used to project on the reference plane or the object under inspection. The projected sinusoidal fringe pattern of varying fringe period can easily be adjusted by setting the value p of the software-generated sinusoidal fringe pattern in Eq. (7).

The proposed LCD-based phase shifting system creates sinusoidal fringe patterns adaptively; it can also shift phase increment accurately. In this study, we adopt the four-step phase shifting method with $\pi/2$ increment (i.e., one fourth of a fringe period). Therefore, accurate phase shifting can be obtained by simply setting the fringe period to a multiple of four. Furthermore, the phase shifting process is conducted by a software-controlled process instead of a physical movement process.

This approach alleviates the limitations of the traditional methods [20-25] that generally perform inaccurate phase shifting by mechanical movements of the PZT or slide projector. The measuring error due to the vibration of mechanical movement and inaccurate phase shifting in conventional methods can be effectively avoided with the proposed scheme.

Figure 2 shows a sketch of the generation and projection of a sinusoidal grating with the proposed technique. Four $\pi/2$ phase-shifted images $F_n(r,c)$ are sequentially generated on the LCD panel, and then projected on the reference plane and captured respectively by the CCD camera. These captured images $I_n(x,y)$ can be used to acquire the reference phase $\phi_r(x,y)$ according to Eq. (5). Similarly, the object (solder paste) phase $\phi_o(x,y)$ can also be obtained with the four $\pi/2$ phase-shifted images. The phase difference $\Delta\phi(x,y)$ of each coordinate (x,y) is then calculated. The surface height $h(x,y)$ of the solder paste under inspection is obtained from Eq. (2). 3D surface profile and volume of the solder paste can be efficiently calculated based on these surface height data in the sensed area.

With a sufficient number of height data values provided by the proposed full-field 3D measurement system, the volume of inspected objects can be obtained by the formula below

$$V = {l_p}^2 * \sum_x \sum_y h(x,y) \tag{8}$$

where l_p represents the associated width of each pixel in *mm*, and $h(x,y)$ is the measured surface height value for each pixel (x,y) within the inspected area.

3.2 System implementation

The implementation of the proposed method for 3D measurement of deposited solder pastes is shown in Figure 3. The most important part in this system is the LCD panel, which has a resolution of 800×600 pixels. This panel is connected to a personal computer, and can be directly controlled by software to generate a transparent sinusoidal grating through an LCD control interface. Since the transparency variation of an LCD panel will be affected by high temperature [27], a cool light source with a power of 150 Watts and a fiber optic light guide are adopted in the system to reduce the transparency variation of the LCD panel. A collimated lens (Lens 1 in Figure 3) with a focal length of 50 *mm* is set up in front of the cool light source to produce collimated light. The collimated light is used to illuminate the software-controlled LCD grating to project the uniform sinusoidal fringe pattern on the object and the rigid flat plate. In this study, the rigid flat plate is used as a reference plane.

A projection lens (Lens 2 in Figure 3) with focal length of 100 *mm* is used to focus the images of the projected sinusoidal fringe patterns onto the rigid flat plate. A precision translation stage with resolution of 0.005 *mm* is used to hold the rigid flat plate and to place the printed circuit board (PCB) under inspection. The collimated lens, the LCD panel, the projection lens and the precision translation stage are all held by optical holders and fixed on a linear optical bench 50 *cm* in length. The angle between the projection axis and the detection axis is 20 degrees. The projected fringe pattern is captured by a CCD camera equipped with a $50\,mm$, $F/1.8$ collocated lens. The sensed image is of 640×480 pixels with 8-bit gray levels.

3.3 Calibration and measurement procedure

The representation of the physical width l_p of a pixel in Eq. (8) and the system parameter *k* in Eq. (2) must be determined prior to the measurement process for a given system setup. In the study, an opal glass with a crossline reticle that has the exactly known width on its surface is first used as the width calibration target to acquire the l_p value in *mm* for each pixel in the sensed image, and then a white flat plate is used as the height calibration target to obtain the system parameter *k*.

It can be seen from Eq. (2) that system parameter *k* can be derived from a known distance d (used as the constant surface height h) divided by its corresponding phase difference, i.e.,

$$k = \frac{h}{\Delta\phi} = \frac{d}{\phi_r - \phi_d} \tag{9}$$

where ϕ_d is the phase function on the white flat plate after the movement d. A simple calibration procedure based on a uniform measurement scale [28] is used to obtain the value *k*. First, the phase function ϕ_r on the white flat plate is determined by the proposed system. Then the precision translation stage that holds the white flat plate is fine-tuned along the vertical z direction with a known distance d (measured in *mm*), as shown in Figure 3. The phase function ϕ_d on the white flat plate after the movement d is then acquired with the proposed system. Following the calibration procedure described above, the system parameter *k* can be obtained according to Eq. (9). The adopted calibration procedure in the proposed system has the advantage that the aberrations of the optical lens, the position of the CCD camera and the projection

angle of the LCD are not necessary to be known and have no effect on the measurement accuracy.

Once the physical width l_p of a pixel in the image and the system parameter *k* are determined, the measurement procedure of the proposed system proceeds as follows.

Step 1. Generate a fringes pattern: The sinusoidal fringe pattern is generated first using Eq. (7) and displayed on the LCD panel.

Step 2. Project sinusoidal fringes: Illuminate the LCD panel with a collimated white light. The sinusoidal fringes pattern image is focused and projected onto the rigid flat plate (the reference plane).

Step 3. Shift phases: The computer-generated sinusoidal fringe pattern that displays on the LCD panel is digitally shifted in four phase steps 0, $\pi/2$, π, and $3\pi/2$.

Step 4. Calculate the reference phase: The intensity images projected on the rigid flat plate are sequentially captured by the CCD camera. Then Eq. (5) is used to compute the phase value $\phi_r(x, y)$ on the rigid flat plate.

Step 5. Calculate the object phase: Place the object to be inspected on the precision translation stage and repeat Steps 3 and 4 to obtain the phase value $\phi_o(x, y)$ in the presence of the object.

Step 6. Compute the surface height: The height value $h(x, y)$ of the object under inspection is acquired with Eq. (2) after the phase difference $\Delta\phi(x, y)$ of each coordinate (x, y) is calculated.

Step 7. Calculate the volume: Once the height value of every pixel in the projected image is measured, the volume of a solder paste can be calculated from Eq.

(8).

4. Experimental results

In this study, a standard 1-*mm* gauge block of grade 0 (the accuracy is ±0.12 *um*) was used to evaluate the measurement capability of the proposed system. The 1-*mm* gauge block was placed on a white flat plate, and the plate is used as the reference plane of the measurement system. Figures 4(a)-(d) show the image of the 1-*mm* gauge block used for testing, the projected image, the range image as an intensity function (the brightness is proportional to the height) and the 3D surface profile of the gauge block. Note that the projected region in Figure 4(b) contains both a partial gauge block and a partial white flat plate so that the desired 1-*mm* surface height can be evaluated and the 3D profile of the step height can be visualized.

The resulting mean step height of the projected area of the gauge block is 1.0058 *mm* and the standard deviation is 0.00831 *mm*. Note that the ideal height of the gauge block is 1 *mm*. To investigate the measurement repeatability, nine equally-spaced points within the projection area of the gauge block, as shown in Figure 4(c), were measured twenty times by the proposed system. The means, the standard deviations and the accuracy of the measured heights for each of the nine test points are summarized in Table 1. The height accuracy of each point is computed by [29]

$$A = \frac{1}{20}\sum_{i=1}^{20}(h_i - \mu_h) \tag{10}$$

where h_i is the measured height and μ_h is the true height value (1 *mm* in this case)

of the standard 1-*mm* gauge block. Table 1 shows that the central point (point number 5) of the projected 1-mm gauge block gives the best accuracy of 0.0010 *mm*, and the smallest standard deviation of 0.0067 *mm*. The table also reveals that the measurement consistency in terms of standard deviation is slightly deteriorated in the left boundary area (point numbers 1, 2 and 3) of the projected gauge block. This is because the sinusoidal fringes in the projected pattern are slightly distorted when they departed from the projection center. However, they are still well measured with an accuracy within 0.0068 *mm* and a standard deviation within 0.0133 *mm*.

In an additional experiment, an area of 6×10 mm^2 of the 1-*mm* gauge block is projected and measured ten times. The projected area of 60 mm^2 corresponds to 68,344 pixels in the image. The ideal volume of the projected gauge block area is 60 mm^3 (i.e. 6×10×1 mm^3). Based on the volume formula of Eq. (8), an average volume of 60.182 mm^3 with standard deviation 0.086 mm^3 is obtained by the proposed system. In terms of the volume measurement of each pixel (volume pixel, voxel), the average voxel is 0.000881 mm^3 and the standard deviation of a voxel is 0.000001 mm^3.

In the experiments, a sample PCB is used to evaluate the efficacy of the proposed 3D measurement system for deposited solder pastes. The test board was a momery module board with printed Sn-Pb solder pastes (Power Quotient International Co., Ltd.). The measured area of the sample PCB solder pastes is marked with the white-dotted frame in Figure 5(a). The height of solder pastes under inspection is 0.1 *mm* on average. A sinusoidal fringe pattern is projected on the measured area, and the projection area is 7×7 mm^2. The width of the computer-generated fringe period is 32 pixels, which corresponds to a projected fringe period of 0.56 *mm* on the inspection object. Figure 5(b) shows the projected fringes image. Figure 5(c) presents the range

image as an intensity function, in which brightness is proportional to the magnitude of surface height. Figure 5(d) shows the 3D surface profile of the inspected solder pastes on the PCB.

This system is capable of measuring the volume of each solder paste. The region of each solder paste can be predetermined from a CAD file of the PCB layout. In this study, we directly separated the regions of individual solder pastes in the resulting height image with a simple segmentation algorithm (thresholding and labeling in image processing). Once the area of each solder paste is determined in the image, the volume of a solder paste can be calculated from Eq. (8).

According to the volume formula of Eq. (8), one of the deposited solder pastes in Figure 5 was measured ten times. An average of 0.161 mm^3 with standard deviation 0.0005 mm^3 is obtained by the proposed system. For comparison purposes, this solder paste was also measured by a laser-based 3D measurement system, and the measured value was 0.160 mm^3.

The proposed system can be easily scaled up to increase the inspection area by moving the projection lens toward the LCD panel. However, the projected fringe period will be correspondingly wider for a given fringe period generated in the LCD panel, and thus reduce the system resolution. In order to maintain good resolution in a large inspection area, we can use a fringe pattern of fine fringe periods. This can be easily achieved by resetting a smaller fringe period on the software-controlled LCD grating. For example, the projection area of the PCB sample shown in Figure 5(a) is changed from 7×7 mm^2 to 14×14 mm^2, and the computer-generated fringe period is reduced from the original setting of 32 pixels to 16 pixels for obtaining the same

width of projected fringe period (0.56 *mm*). Figures 6(a)-(d) show the measurement result of the sample PCB in the larger projection area of 14×14 mm^2.

Volume measurement of the same inspected solder pastes is also performed in larger areas. Table 2 summarizes the means and standard deviations of the measured volume under different projection areas and fringe periods. It can be seen from Table 2 that the resulting statistics for the PCB sample in a smaller projection area (Figure 5(a)) and in a larger projection area (Figure 6(a)) are approximately equal, even though the projection area is increased by 400%. The measurement repeatability in terms of standard deviation is slightly deteriorated from 0.0005 mm^3 to 0.0006 mm^3 when the projection area is increased from 7×7 to 14×14 mm^2. A fine fringe period generally yields better measurement resolution. However, it should be noticed that the fringe period cannot be reduced unconditionally. When the fringe period becomes smaller, the fringe contrast will also be reduced and may result in insufficient signal-to-noise data points.

Besides the adaptability in the generation of fringe patterns, the efficiency of the proposed system in the 3D measurement can also be demonstrated by the above measured data. Although the projection area in Figure 6 is four times of that in Figure 5, the measuring time is the same in the experiments. The reason is that the proposed system performs full-field 3D measurement as long as the projection area is within the field of view (FOV) of a CCD camera. This is the merit of the proposed full-field 3D measurement system. In the experiments, the processing time of the proposed 3D measurement scheme for an image of 640×480 pixels is less than 1 second on a Pentium Ⅳ 1.4-GHz personal computer (PC).

Under the condition of a 0.36x capturing lens and a Pentium Ⅳ 1.4-GHz PC, the physical area of 160×100 mm^2 corresponds to 18,225,000 measuring points (5,400 ×3,375 pixels) in images. The computation time of this system to check a typical 160× 100 mm^2 PCB for the paste volume is less than 45 seconds if every pixel of the whole PCB image is evaluated. The computation time of this system can be further reduced with a higher performance PC. This system can also be equipped with a fast and precise x-y motion stage to automatically complete the paste volume measurement of the 160×100 mm^2 PCB.

5. Conclusions

In this paper, a fast 3D measurement system for deposited solder pastes is presented. The proposed system integrates a software-controlled LCD grating and an incoherent light source to generate the required sinusoidal fringe pattern and to obtain accurate shift phase. It avoids measuring errors from the laser speckle effect and inaccurate phase shifting in the application of solder volume measurement. The proposed system can perform full-field 3D measurement of solder pastes in an area. This area-measuring approach can speed up the volume measurement of solder pastes, compared to the line-scanning scheme of laser-based systems. Furthermore, the proposed system can be easily adjusted to scale up an inspection area. Experiments from real sample PCB solder pastes have shown that the 3D profiling and volumes measured by the proposed system are efficient and effective. Table 3 shows the comparisons of accuracy and speed among the proposed technique and the existing 3D measurement techniques.

In this study, a fixed value of the system parameter k is used to derive the height

of every pixel in the projected image. The calibrated k parameter allows a measurement without knowing the off-axis alignment error and lens distortion. For more accurate measurement of the height in varying coordinates of the projected image, an adaptive k approach that uses a matrix $k(x, y)$ to store the corresponding k value at each individual pixel (x, y) location is currently under investigation.

6. Acknowledgements

We acknowledge financial support from National Science Council of Taiwan, ROC and Horng Terng Automation Co., Ltd. We also thank the reviewers for their helpful comments.

References

1. I. Fidan, R. P. Kraft, L. E. Ruff, and S. J. Derby, “Designed experiments to investigate the solder joint quality output of a prototype automated surface mount replacement system,” *IEEE Transaction on Components, Packaging, and Manufacturing Technology-Part C*, vol. 21, pp. 172-181,1998.
2. D. He, N. N. Ekere and M. A. Currie, “The behavior of solder pastes in stencil printing with vibrating squeegee,” *IEEE Transactions on Components, Packaging, and Manufacturing Technology-Part C*, vol. 21, pp. 317-324, 1998.
3. S. C. Richard, “The complete solder paste printing processes,” *Surface Mount Technology*, vol. 13, pp. 6-8, 1999.
4. J. Pan, G. L. Tonkay, R. H. Storer, R. M. Sallade and D. J. Leandri, “Critical variables of solder paste stencil printing for micro-BGA and fine pitch QFP,” *Proceedings of IEEE/CPMT International Electronics Manufacturing Technology Symposium*, pp. 94-101, 1999.
5. D. W. Capson and S. K. Eng, “A tiered-color illumination approach for machine inspection of solder joints,” IEEE Trans. Pattern Analysis Mach. Intell., vol. 10, pp. 387-393, 1988.
6. K. W. Ko, H. S. Cho, J. H. Kim and J. S. Kim, “Solder joints inspection using neural network and fuzzy rule-based classification,” *Proceedings of the IEEE/RSJ Intl. Conference on Intelligent Robots and Systems*, pp. 1565-1570, October, Victoria, B. C. Canada, 1998.
7. T. H. Kim, T. H. Cho, Y. S. Moon and S. H. Park, “Automatic inspection of solder joints using layered illumination,” IEEE Intl. Conference on Image Processing, 2, 645-648, Sept. 16-19, 1996.
8. J. Morini, J. Cronin and O. O'Neal, “Optimizing printer-based solder paste inspection,” *Circuits Assembly*, vol. 13, pp. 32-37, 2002.
9. M. Owen, “2-D and 3-D inspections catch solder-paste problems,” *Test and Measurement World*, vol. 20, pp. 13-18, 2000.
10. Y. P. Wu, P. L. Tu and Y. C. Chan, “The effect of solder paste volume and reflow ambient atmosphere on reliability of CBGA assemblies,” *Journal of Electronic Packaging*, vol. 123, pp. 284-289, 2001.
11. R. R. J. Lathrop, “Solder paste print qualification using laser triangulation,” *IEEE Transactions on Components, Packaging, and Manufacturing Technology*, vol. 20,

pp. 174-182, 1997.

12. T. Okura, M. Kanai, S. Ogata, T. Takei and H. Takakusagi, “Optimization of solder paste printability with laser inspection technique,” *Proceedings of IEEE/CPMT International Electronics Manufacturing Technology Symposium*, pp. 361-365, 1997.
13. E. H. Rideout, “Lowering test costs with 3-D solder-joint inspection,” *Test and Measurement World*, vol. 10, pp. 744-1657, 1990.
14. Ryu, Y. K. and H. S. Cho, 1997, “New optical measuring system for solder joint inspection,” *Optics and Lasers in Engineering*, Vol. 26, pp. 487-514.
15. H. Tsukahara, Y. Nishiyama, F. Takahashi, T. Fuse, M. Ando and T. Nishino, “High-speed 3D inspection system for solder bumps,” *Proceedings of SPIE*, vol. 2597, pp. 168-177, 1995.
16. J. L. Horijon, W. D. Amstel, F. C. Couweleer and W. C. Ligthart, “Optical system of an industrial 3D laser scanner for solder paste inspection,” *Proceedings of SPIE*, vol. 2599, pp. 162-170, 1995.
17. S. Tang and Y.Y. Hung, “Fast profilometer for the automatic measurement of 3-D object shapes,” *Applied Optics*, vol. 29, pp. 3012-3018, 1990.
18. X. Y. Su, W. S. Zhou, G. V. Bally and D. Vukicevic, “Automated phase-measuring profilometry using defocused projection of a Ronchi grating,” *Optics Communications*, vol. 94, pp. 561-573, 1992.
19. H. Zhao, W. Chen and Y. Tan, “Phase-unwrapping algorithm for the measurement of three-dimensional object shapes,” *Applied Optics*, vol. 33, pp. 4497-4500, 1994.
20. V. Srinivasan, H. C. Liu and M. Halioua, “Automated phase-measuring profilometry of 3-D diffuse objects,” *Applied Optics*, vol. 23, pp. 3105-3108, 1984.
21. S. Toyooka and Y. Iwaasa, “Automatic profilometry of 3-D diffuse objects by spatial phase detection,” *Applied Optics*, vol. 25, pp. 1630-1633, 1986.
22. G. Mauvoisin, F. Bremand, and A. Lagarde, “Three-dimensional shape reconstruction by phase shifting shadow moiré,” *Applied Optics*, vol. 33, pp. 2163-2169, 1994.
23. B. V. Dorrio and J. L. Fernandez, “Phase-evaluation methods in whole-field optical measurement techniques,” *Measurement Science*, vol. 10, pp. 33-55, 1999.
24. V. Srinivasan, H. C. Liu and M. Halioua, “Automated phase-measuring

profilometry: a phase mapping approach," *Applied Optics*, vol. 24, pp. 185-188, 1985.

25. T. Xian and X. Su, "Area modulation grating for sinusoidal structure illumination on phase-measuring profilometry," *Applied Optics*, vol. 40, pp. 1201-1206, 2001.
26. J. E. Greivenkamp and J. H. Bruning, "Phase shifting interferometry, " in *Optical Shop Testing*, D. Malacara (ed.), Wiley, New York, 1992.
27. F. Docchio, G. Sansoni and N. Viviani, "Light-induced transmission changes in liquid crystal displays for adaptive pattern projection," *IEEE Transactions on Instrumentation and Measurement*, vol. 41, pp. 629-632, 1992.
28. A. Asundi and W. Zhou, "Unified calibration technique and its applications in optical triangular profilometry," *Applied Optics*, vol. 38, pp. 3556-3561, 1999.
29. Y. R. Shiau and B. C. Jiang, "Determine a vision system's 3D coordinate measurement capability using taguchi methods," *International Journal of Production Research*, 29, pp. 1101-1122, 1991.

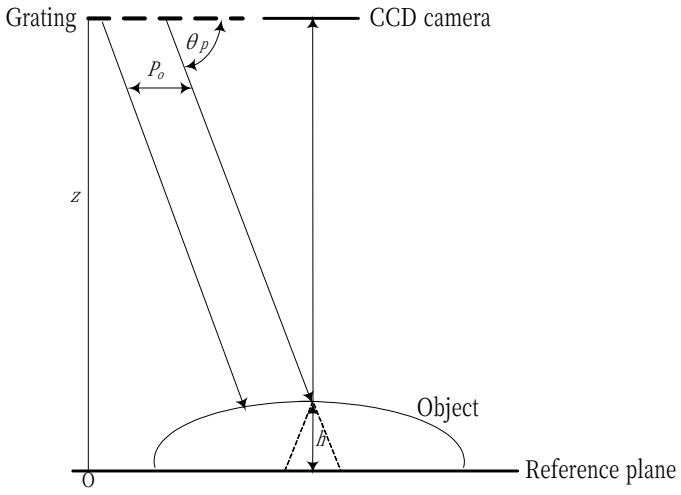

Fig. 1. Optical geometry of the phase measuring method.

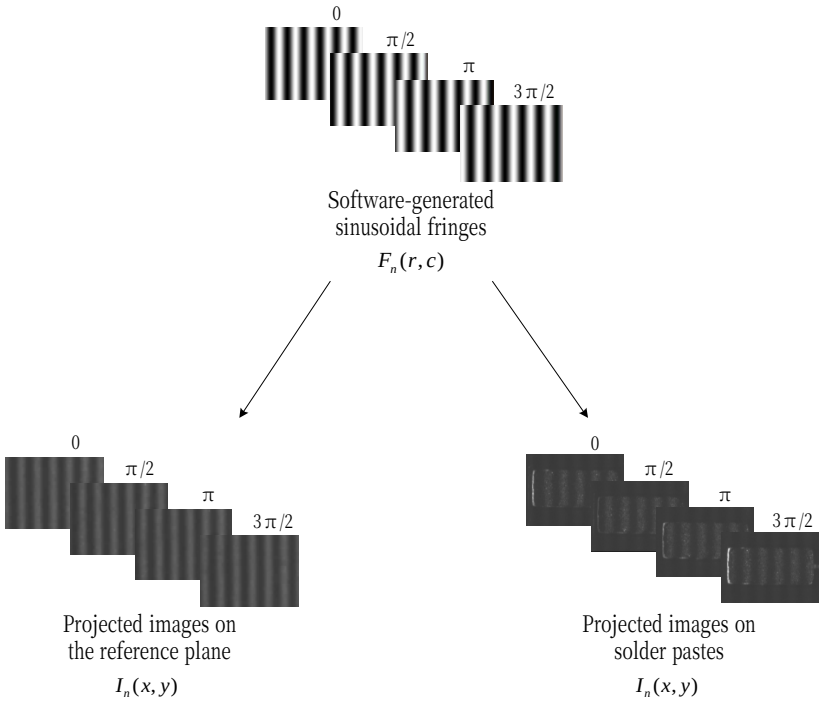

Fig. 2. Sketch of the generation and projection of sinusoidal grating with LCD-based phase shifting techniques.

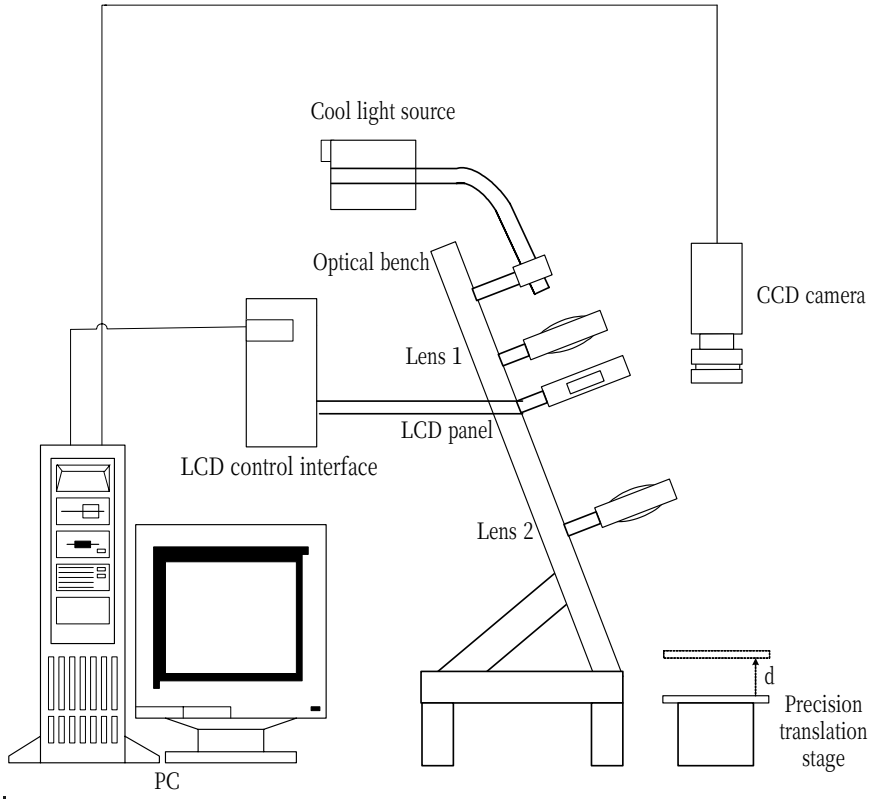

Fig. 3. System implementation of the proposed 3D measurement scheme.

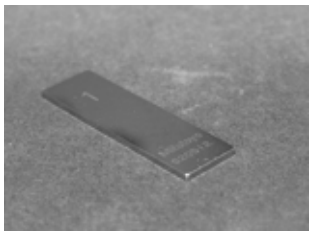

(a)

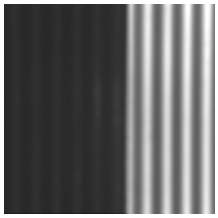

(b)

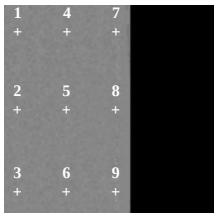

(c)

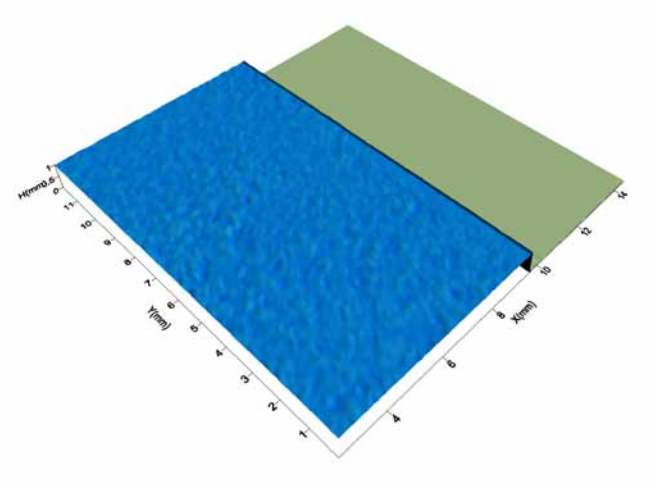

(d)

Fig. 4. The measurement of a standard 1-*mm* gauge block from the LCD-based system: (a) the 1-*mm* gauge block used for testing; (b) projected image; (c) range image as an intensity function, where brightness is proportional to the magnitude of the measured height (The numbers mark nine equally-spaced points measured twenty times by the proposed system); (d) 3D surface profile.

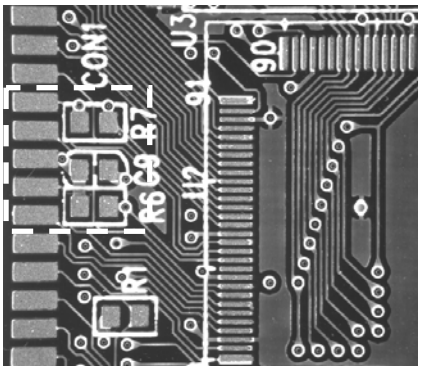

(a)

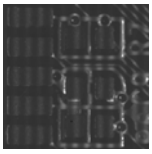

(b)

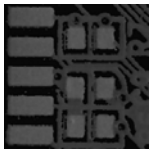

(c)

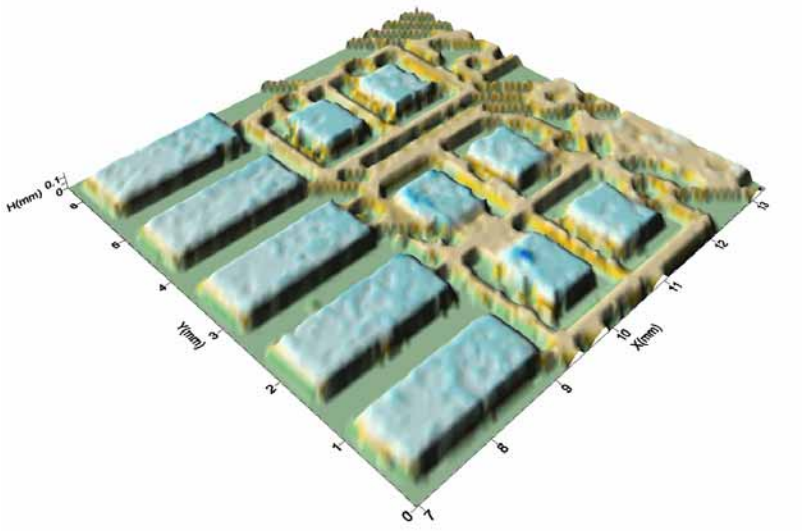

(d)

Fig. 5. Sample PCB solder pastes in a projection area of 7×7 mm^2: (a) original image; (b) projected image with the fringe period of 32 pixels; (c) range image as an intensity function; (d) 3D surface profile.

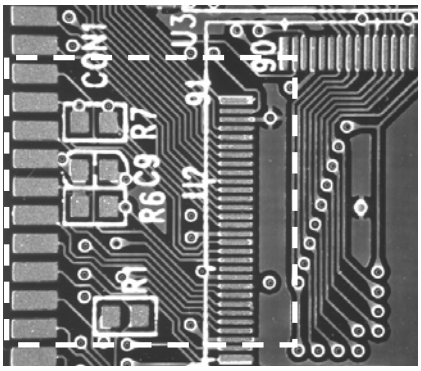

(a)

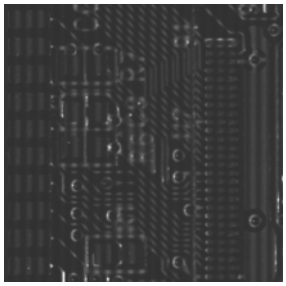

(b)

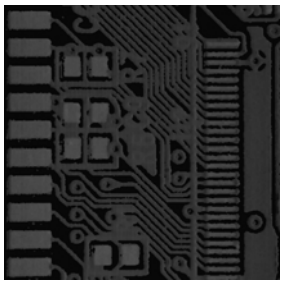

(c)

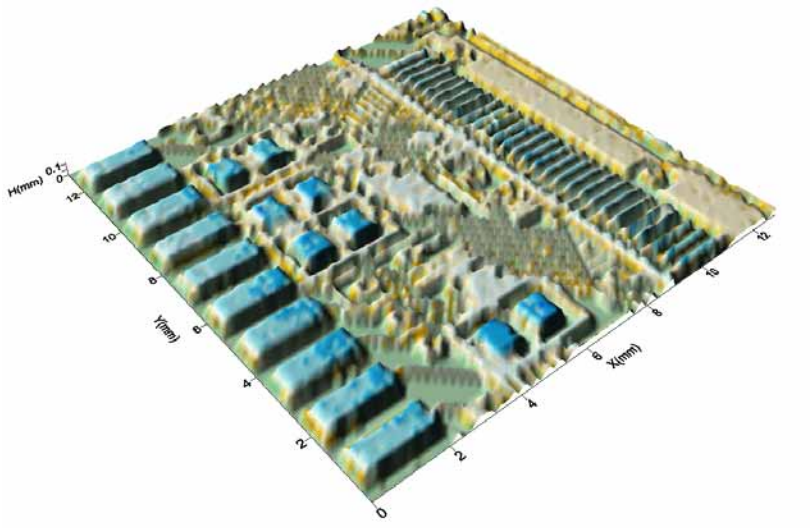

(d)

Fig. 6. Sample PCB solder pastes in a larger projection area of 14×14 mm^2: (a) original image; (b) projected image with the fringe period of 16 pixels; (c) range image as an intensity function; (d) 3D surface profile.

Table 1. Measurement consistency and accuracy for the 1-*mm* gauge block from the LCD-based system.

Point number	1	2	3	4	5	6	7	8	9
Mean (*mm*)	0.9937	1.0068	0.9943	0.9957	1.0010	1.0066	0.9940	0.9947	1.0072
Standard deviation (*mm*)	0.0133	0.0102	0.0120	0.0074	0.0067	0.0069	0.0078	0.0077	0.0077
Accuracy (*mm*)	-0.0063	0.0068	-0.0057	-0.0043	0.0010	0.0066	-0.0060	-0.0053	0.0072

Note: 1. The statistics of each point are based on 20 repetitive measurements.

2. The point numbers correspond to the locations marked in Figure 4(b).

Table 2. Comparisons of measured results under different projection areas and fringe periods.

Solder paste sample	Mean (mm^3)	Standard deviation (mm^3)
Fig. 5 Projection area = 7×7 mm^2 Computer-generated fringe period = 32 pixels	0.161	0.0005
Fig. 6 Projection area = 14×14 mm^2 Computer-generated fringe period = 16 pixels	0.163	0.0006

Note: The resulting statistics are based on 10 repetitive measurements.

Table 3. Comparisons of accuracy and speed among the proposed technique and the popular optical 3D measurement techniques.

Attribute / Measurement technique	Accuracy (height measurement)	Speed (measured points per second)
Optical focus technique	>1 *um*	<60K points /s
Laser scanning technique	>2 *um*	<100K points /s
Proposed technique	>5 *um*	>200K points /s